Pergamon

PII: S0301-9322(96)00026-2

Int. J. Multiphase Flow Vol. 22, No. 5, pp. 849–861, 1996

0301-9322/96 $15.00 + 0.00

EXPERIMENTAL STUDY OF A TWO-PHASE BUBBLY FLOW IN A FLAT DUCT SYMMETRIC SUDDEN EXPANSION—PART II: LIQUID AND BUBBLE VELOCITIES, BUBBLE SIZES

F. ALOUI and M. SOUHAR

LEMTA (CNRS URA-875)-ENSEM-INPL. 2, Avenue de la Forêt de Haye, 54516, Vandœuvre-Lès-Nancy, France

(Received 20 December 1994; in revised form 17 March 1996)

Abstract—Experimental results obtained in a gas–liquid bubbly flow in a flat horizontal sudden expansion are presented in this study and constitute useful data for the numerical code. The use of hot film anemometry in the continuous phase (liquid) of a bubbly flow allows a determination of the average and fluctuating velocity. For the dispersed phase, the use of a double optical probe allows the determination of the average and fluctuating axial velocity and the granulometry of the bubbles. A comparison of these quantities with the results obtained by a fast video camera shows very good agreement. The different measuring quantities were discussed and an organization scheme of the flow in a sudden expansion was proposed. Copyright © 1996 Elsevier Science Ltd.

Key Words: bubbly flow, plane sudden expansion, axial liquid phase velocity, axial bubble velocity, granulometry of bubbles, visualization of bubbly flow by fast video camera

1. INTRODUCTION

In part I, a qualitative and quantitative study of a bubbly flow downstream of a two-dimensional sudden expansion was presented. The qualitative study by visualization pointed out the phenomenon of dissymmetry of the flow at low volumeric qualities and the transition towards a quasi-symmetric flow at void fractions above 10%. The quantitative study was practically limited to symmetric bubbly flows, and involved the evolution of the pressure and the local and average void fraction downstream of the singularity.

With regards to the dynamics of bubbly flow in two-dimensional sudden expansions, one observes the absence of experimental data on local velocities relative to each phase as well as the granulometry of bubbles. Recent works carried out by Bel Fdhila (1991), Bel Fdhila & Simonin (1992) involved only the velocity of the liquid phase in axisymmetrical sudden expansions. It is therefore considered useful in this work to constitute a somewhat complete data bank on this type of flow. These results will serve as data for local models and help to describe the organization of bubbly flow in this configuration.

This second part will centre on the dynamics of the flow in each of the two phases. To achieve this, the different average and fluctuating velocities relating to the continuous and dispersed phases are determined. These magnitudes are completed by local data of granulometry of bubbles downstream of the singularity. The jet line separating the principal flow from the recirculation regions is then determined as well as the general reorganization of the bubbly flow downstream of the sudden expansion.

Belakhovsky's model (1966) was used in calculating the bubble sizes. This model had been verified by the experimental data of Galaup (1975), and used by Herringe & Davis (1976), Clark & Turton (1988) and recently by Liu (1993). A fast video camera EKTAPRO was also used to determine the axial velocity profiles and the granulometry of the bubbles as an additional control of the double optical probe measurements.

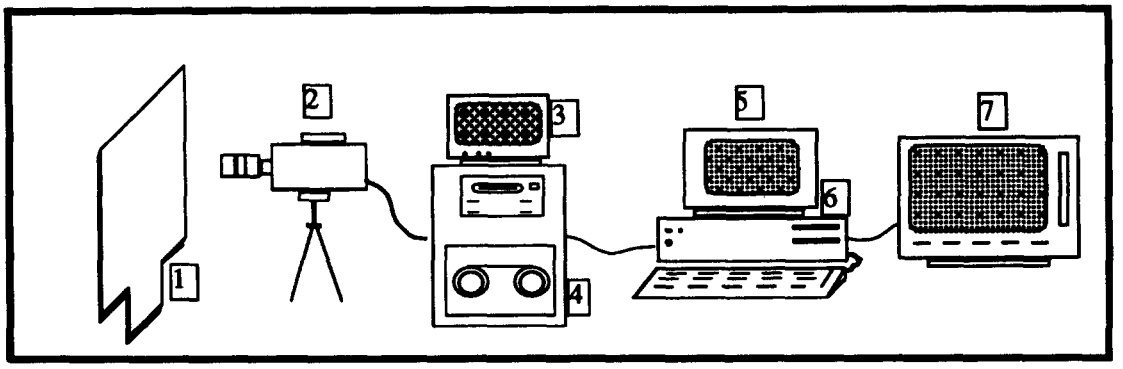

Figure 1. Schematic apparatus of the bubbly flow visualization: 1: flat sudden expasion; 2: video camera; 3 and 7: monitors 4: cassette recorder; 5 micro-computer; 6: cyclope card.

2. EXPERIMENTAL AND MEASURING DEVICE

The experimental device used is composed of two circuits: a "closed" liquid circuit and an "open" gas circuit which feeds a test section made of transparent plexiglas. The test section has rectangular cross sections of $44 \times 5\ mm^2$ upstream and $100 \times 5\ mm^2$ downstream of the expansion. This experimental set up and the metrology used are described in details in the first part (part I).

The visualization system used in part II (figure 1) is composed of a video camera CCD (Ektapro 1000) equipped with several lenses, a video recorder, a cassette conditioner, a mini control console and a monitor. This unit enables the filming of phenomena up to 1000 frames/s on a full screen, and 6000 images/s per subdivision of the screen. The resolution is 240/192 pixels with a vertical contraction of the image to be corrected during processing. The processing of the images was ensured by a PC micro-computer, a digitilization card (Cyclope), an image processing software (Esilab), and a laser printer for the printing of the images on paper. The acquisition of the images by means of the cyclope card is made directly from the Kodak EKTAPRO recorder.

3. RESULTS AND DISCUSSIONS

3.1. Upstream of the expansion

The axial velocity profiles for both liquid and gas phases and for the different couples of liquid and gas flowrates were measured at the upstream side of the singularity. Calculation of liquid and gas flowrates (the same as in part I) by the integration of these profiles leads to a relative deviation of at most 5% between the operating liquid and gas flowrates and those calculated. This constitutes a good control of the processing procedure of the signals obtained from the hot film probe.

Figure 2 shows that the axial velocity profiles of the liquid phase $\bar{u}_L$ and of the dispersed phase $\bar{u}_\ell$ are almost flat across the whole section. However, one can observe the existence of two peaks in the vicinity of the side walls for $\bar{u}_L$. Also, it is observed that measurements of $\bar{u}_\ell$ by the fast video camera EKTAPRO (4000 frames/s) are very close to those measured by the double optical probe. This shows that the velocity $\bar{u}_\ell$ is correctly measured by the double optical probe. We can also note that the values of the slip velocity $(u_\ell - u_r)$ are the same as the values calculated in part I (in upstream ≈ 0.8 m/s and 0.2 m/s in downstream: see figures 2 and 9a).

The cutting lengths of the bubbles ℓ_ℓ and the velocities $\bar{u}_\ell$ were measured simultaneously. In order to get a correct estimation of the bubble diameters D_ℓ, different acquisition periods were tested to obtain the probability density $\mathcal{P}(\ell_\ell)$, and it was observed that when the number of bubbles are greater than or equal to about 150, the different $\mathcal{P}(\ell_\ell)$ curves converge towards the presumed probability density. The curve $\mathcal{P}(\ell_\ell)$ is used to establish the profile of D_ℓ. This profile is almost uniform and is comparable to the results obtained by the fast video camera (figure 2). The order of magnitude of the bubble diameters is about 5 to 6 mm. This means that the bubbles touch the walls, and this is problematic for the choice of the drag coefficients C_D (see part I).

The fluctuation rates for each of the two phases are presented in figure 3. The latter appear almost the same for the liquid and the gas and can reach values of about 23%. As far as the symmetry

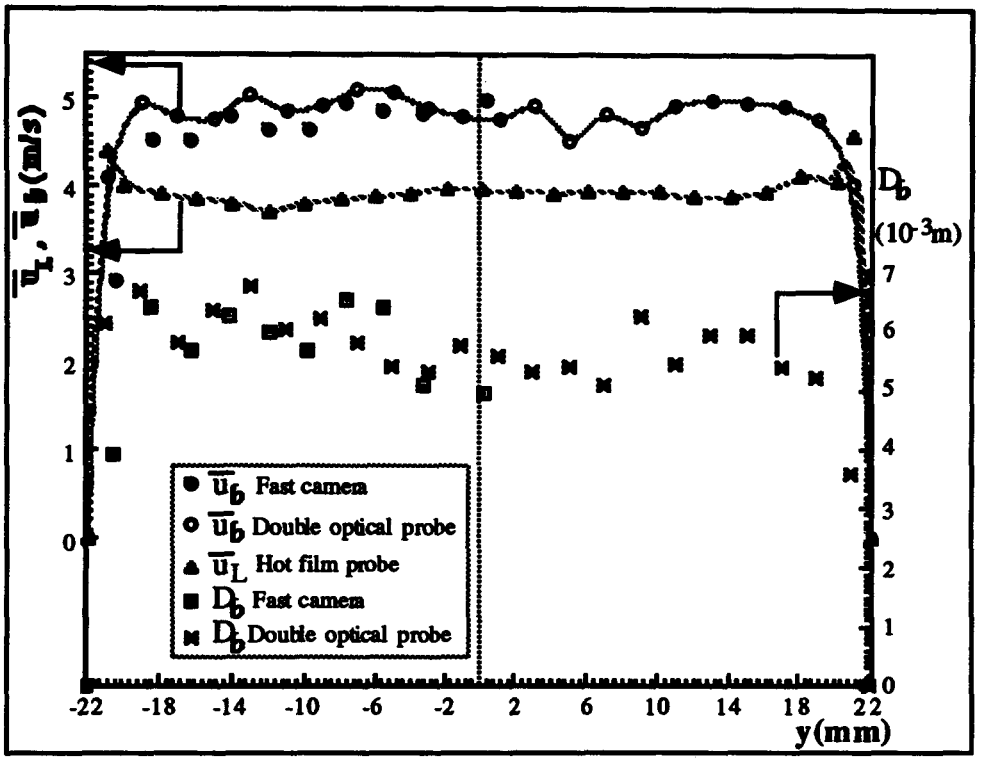

Figure 2. Profiles of the axial liquid and bubble velocities and the bubble granulometry in upstream ($\zeta = -0.35$): comparison between the results obtained by fast video camera and those obtained by double optical probe for $U_{LSI} = 3.2$ m/s and $x = 20.8\%$.

of the two profiles is concerned, it seems almost assured. Compared with a single-phase flow (liquid only) profile, these fluctuation rates are nearly four times higher than those obtained in single-phase flow (Aloui & Souhar 1994). This is not surprising because the presence of the dispersed phase increases the agitation of the liquid phase. The increase of $\sqrt{\overline{u_L'^2}}$ is due to pseudo-turbulence and $\sqrt{\overline{u_L'^2}} \approx (u_\ell - u_\ell)$ according to the rule of thumb. This is verified by our measurements: $\sqrt{\overline{u_L'^2}} \approx 0.8$ m/s and $(u_\ell - u_\ell) \approx 0.8$ m/s.

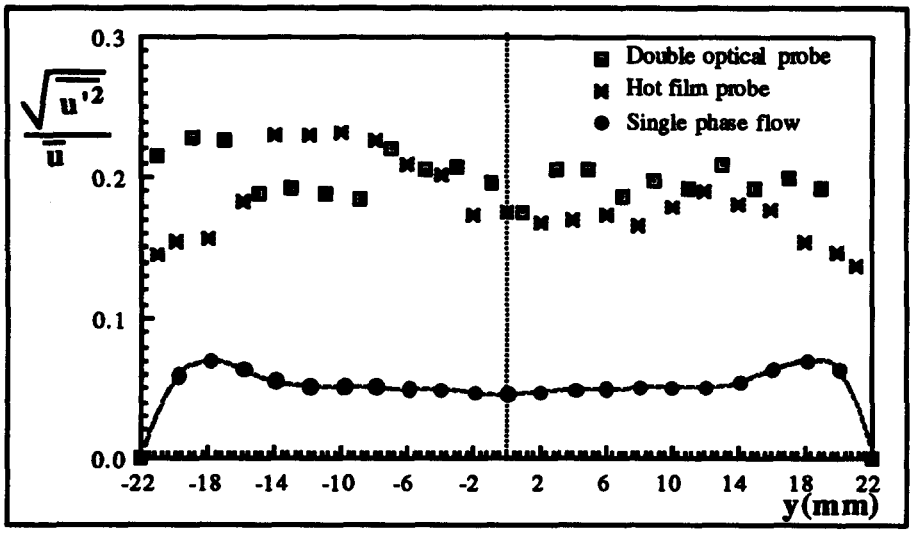

Figure 3. Profiles of the axial fluctuation rates of liquid and gas phases upstream of the sudden expansion ($\zeta = -0.35$) for $U_{LSI} = 3.2$ m/s and $x = 20.8\%$.

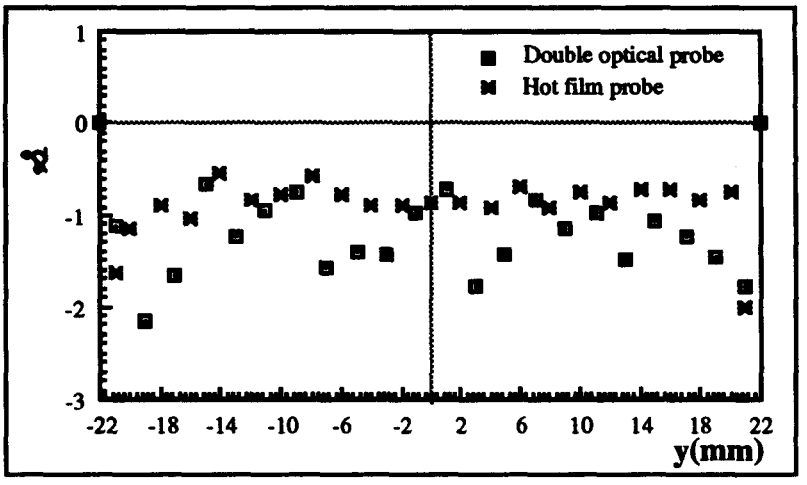

Figure 4. Skewness factor profiles of liquid and gas phases upstream of the sudden expansion ($\zeta = -0.35$) for $U_{LSI} = 3.2$ m/s and $x = 20.8\%$.

The skewness factor $\mathscr{S}$ $(=\bar{u}'^3/(\bar{u}'^2)^{3/2})$ varies from -0.6 to -2 for both liquid and gas phases (figure 4). This variation shows the existence of big puffs at the lower side of the two centred signals. The flatness factor $\mathscr{F}$ $(=\bar{u}'^4/(u'^2)^2)$ of each of the two phases (figure 5) shows a big difference between the continuous phase and the dispersed phase. In the case of the gas, the value of this factor is about 3. Whereas, for the case of the liquid, the normalized histograms become widespread and consequently lead to the increase of $\mathscr{F}$. This can be attributed to the high variations of the liquid velocity in the immediate vicinity of the bubble. Let us remember that the measurements of high order moments ($\mathscr{S}$ and $\mathscr{F}$) are extremely sensitive to the discrimination process; and consequently, the values of $\mathscr{S}$ and $\mathscr{F}$ given here represent only an order of magnitude.

3.2. *Downstream of the expansion*

The evolution of the average axial velocity $\bar{u}_L$ and the average axial velocity $\bar{u}_\ell$ against the dimensionless distance ζ downstream of the sudden expansion is plotted in figure 6. In contrast with single-phase flow (Aloui 1994), the axial velocity profiles $\bar{u}_L$ ($y \leqslant 0$ and $y \geqslant 0$) in different sections are symmetrical about the axis of the expansion (figure 6a). As a result of this symmetry, the axial velocities of the bubbles $\bar{u}_\ell$ were measured only in one half of the test section (figure 6b).

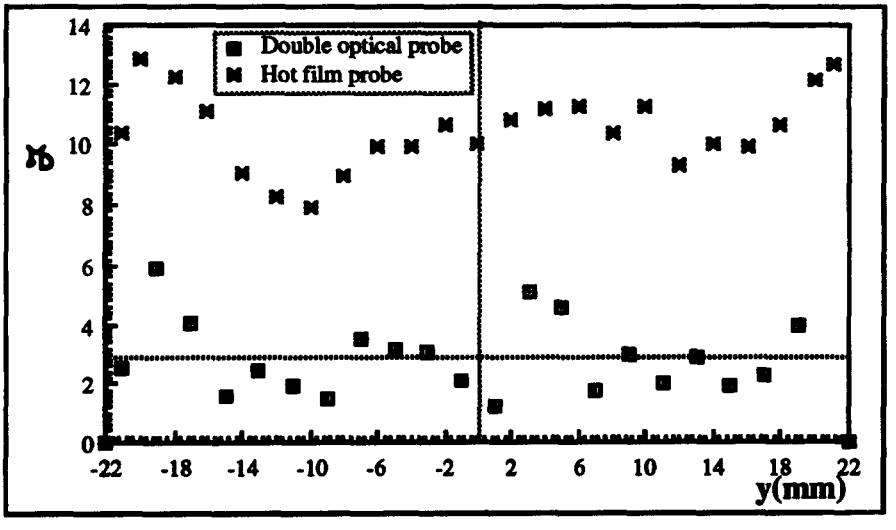

Figure 5. Flatness factor profiles and gas phases upstream of the sudden expansion ($\zeta = -0.35$) for $U_{LSI} = 3.2$ m/s and $x = 20.8\%$.

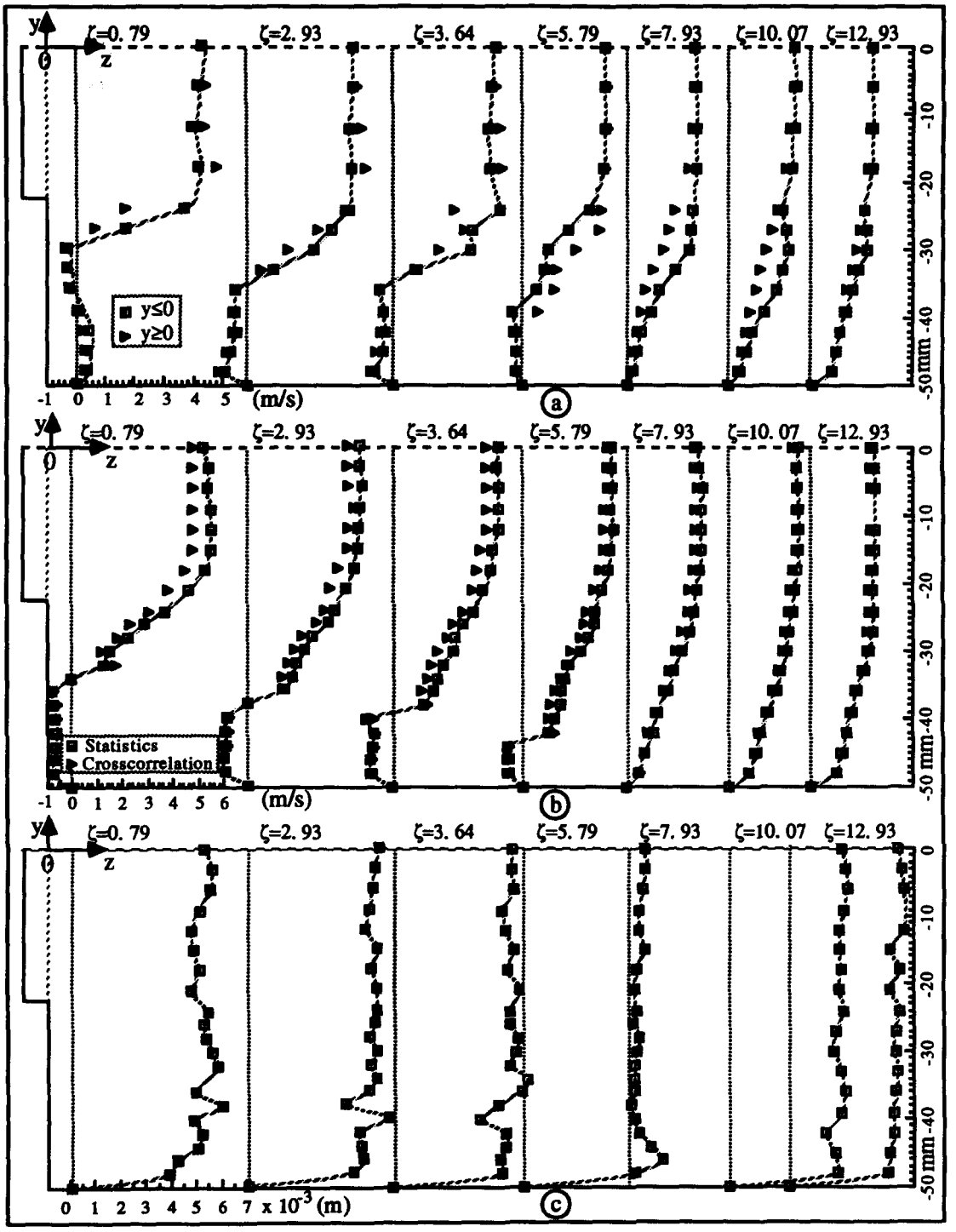

Figure 6. Evolution of the axial velocity of liquid (a), the axial velocity of bubbles (b) and the granulometry of bubbles (c) downstream of the sudden expansion for $U_{LSI} = 3.2$ m/s and $x = 26.7\%$.

An examination of the shape of the different profiles (liquid and gas) shows that the axial velocity passes progressively from a nearly flat shape at the entrance to a power–law shape at the exit from the singularity. The axial velocity profiles of the bubbles $\bar{u}_\ell$ plotted in figure 6b were obtained by statistical calculation (see part I) and by temporal cross correlation of the two optical signals. The first observation (abvious) is that the recirculation region downstream of the expansion presents a reverse flow which results in negative velocities of $\bar{u}_\ell$ near the side wall. The profile of $\bar{u}_\ell$ is almost

flat in the reverse flow and possesses high gradients in the vicinity of $\bar{u}_\ell = 0$. Along each streamline, the presence of a sudden expansion causes a progressive reduction of the bubble velocities outside the regions of vortices. A series of profiles of diameters D_ℓ for different dimensionless distances ζ are also presented in figure 6c. The first observation which can be made is that the diameters remain almost constant across each section. Within the jet immediately at the entrance (up to $\zeta = 4$) the diameters are similar to those found upstream. Beyond $\zeta = 4$ and outside the vortex region, the local size of bubbles decreases progressively when the velocity decreases up to the establishment of the flow farther away from downstream of the singularity.

The profiles of the standard deviation ($\sqrt{\bar{u}'^2}$) downstream of the singularity are given by figure 7 for both the liquid and gas phases. In the main flow, the variation of the standard deviation is practically uniform. On the other hand, in the vortex regions, and particularly, in mixing regions with high velocity gradients, the fluctuating flow is very much disturbed. In the liquid phase however one can observe the existence of maximum values of ($\sqrt{\bar{u}_L'^2}$) which are symmetrical about the axis of the singularity ($y \leqslant 0$ and $y \geqslant 0$) as shown by figure 7a. The variation of the standard deviation in the small vortices is very small. These results are comparable to those obtained by Bel Fdhila & Simonin (1992) in an axisymmetrical sudden expansion configuration.

Concerning the fluctuation of the axial velocity of the bubbles ($\sqrt{\bar{u}_\ell'^2}$) in the principal flow in the downstream side of the singularity, the value of $\sqrt{\bar{u}_\ell'^2}$ is considerable and remains almost constant (figure 7b). This reduces progressively as one moves farther away from the expansion. This decrease is similar to that of the axial velocity ($\sqrt{\bar{u}_\ell'^2}$) and a little different from ($\sqrt{\bar{u}_L'^2}$). In the recirculation region, it is observed that the zones which have few bubbles are the regions of

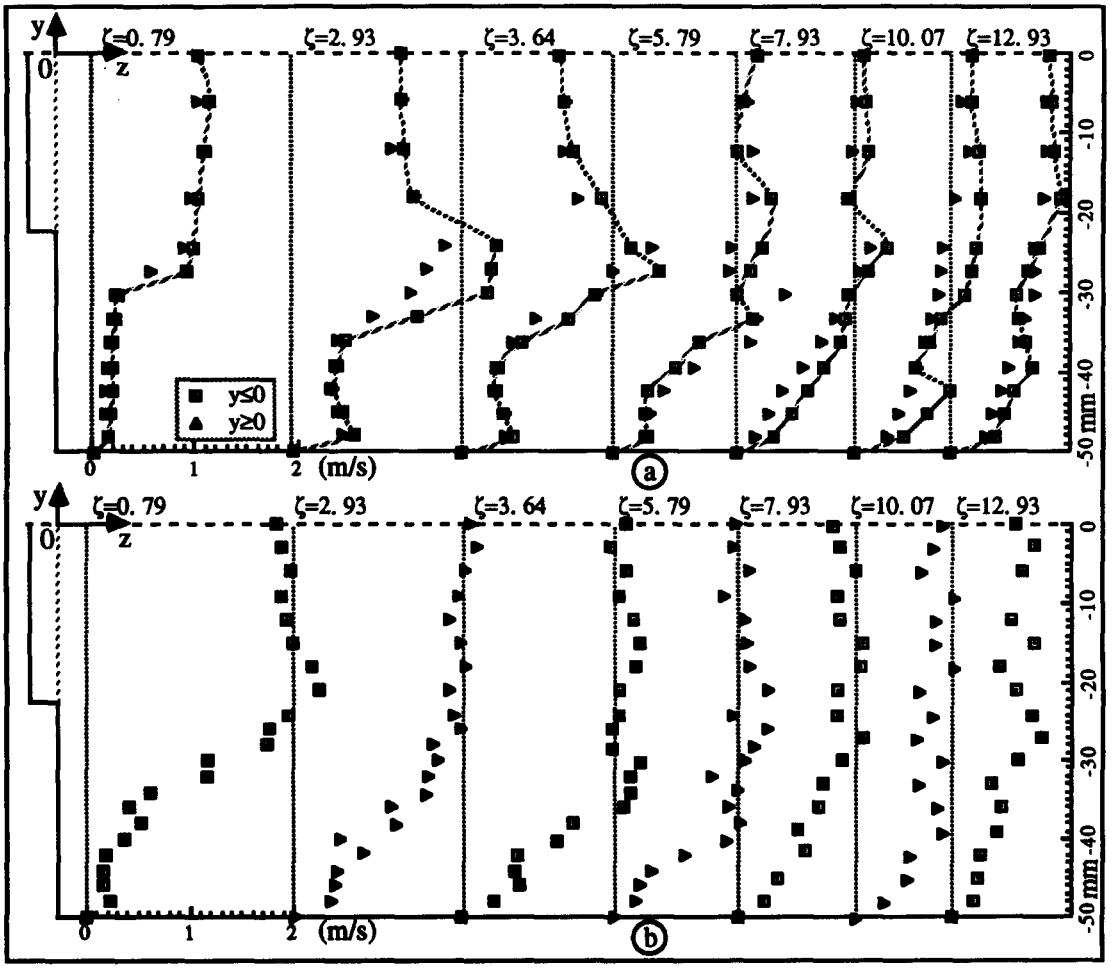

Figure 7. Evolution of the standard deviation $\sqrt{\bar{u}'^2}$ downstream of the sudden expansion for $U_{LSI} = 3.2$ m/s and $x = 26.7\%$: (a) liquid phase, (b) dispersed phase.

low "turbulence". Beyond vortex regions, the profiles of ($\sqrt{\bar{u}_l'^2}$) become nearly constant across the whole section.

In the upstream side of the singularity, the real images of the direct visualization of the flow was superposed on the lines of iso-skewness factor $\mathscr{S}$ (figure 8a) and iso-flatness factor $\mathscr{F}$ (figure 8b) plotted with the same scale. It is observed that the streamlines of the different vortices (visualization) superpose well on the lines of iso-coefficients of $\mathscr{S}$ and $\mathscr{F}$. In addition, the absolute values of these coefficients (skewness and flatness factors) increase progressively as one goes closer to the axes of the big vortices. Lastly, it is observed that oval and concentric lines of iso-coefficients end in the neighbourhood of $\zeta = 7$ to 8; which corresponds to the reattachment points.

The influence of disturbances provoked by the bubbles, on the skewness $\mathscr{S}$ and flatness $\mathscr{F}$ factors is also analysed. For the skewness factor $\mathscr{S}$ (figure 8a), the bubbly flow (highly turbulent) is influenced by turbulent puffs at the negative side of the centred velocity signal relative to the liquid phase only. According to figure 8a, this coefficient varies monotonically along the axis of the expansion, and the values of $\mathscr{S}$ are very much lower than those in a one-phase turbulent flow. Effectively, the very small bubbles in the wake of bigger ones modify slightly the local heat transfer on the hot wire. This modification provokes small negative puffs of the signal without necessarily reaching the threshold fixed during processing (cf. part I). Taking into consideration the type of threshold used for processing this type of flow, the amplitude of the fluctuations of the signal of the continuous phase is slightly amplified in the negative side. This amplification is then manifested by the decrease of the skewness factor which can even reach -1.6 at the centres of vortices. The flatness factor $\mathscr{F}$ which characterizes the intermittence of the flow along the centre of the expansion (figure 8b), shows also that the "turbulence" studied is far from a classical situation. The latter increases when the void fraction increases. In single-phase flow, this factor is about 3. Whereas in bubbly flow, this factor is of the order of 8.

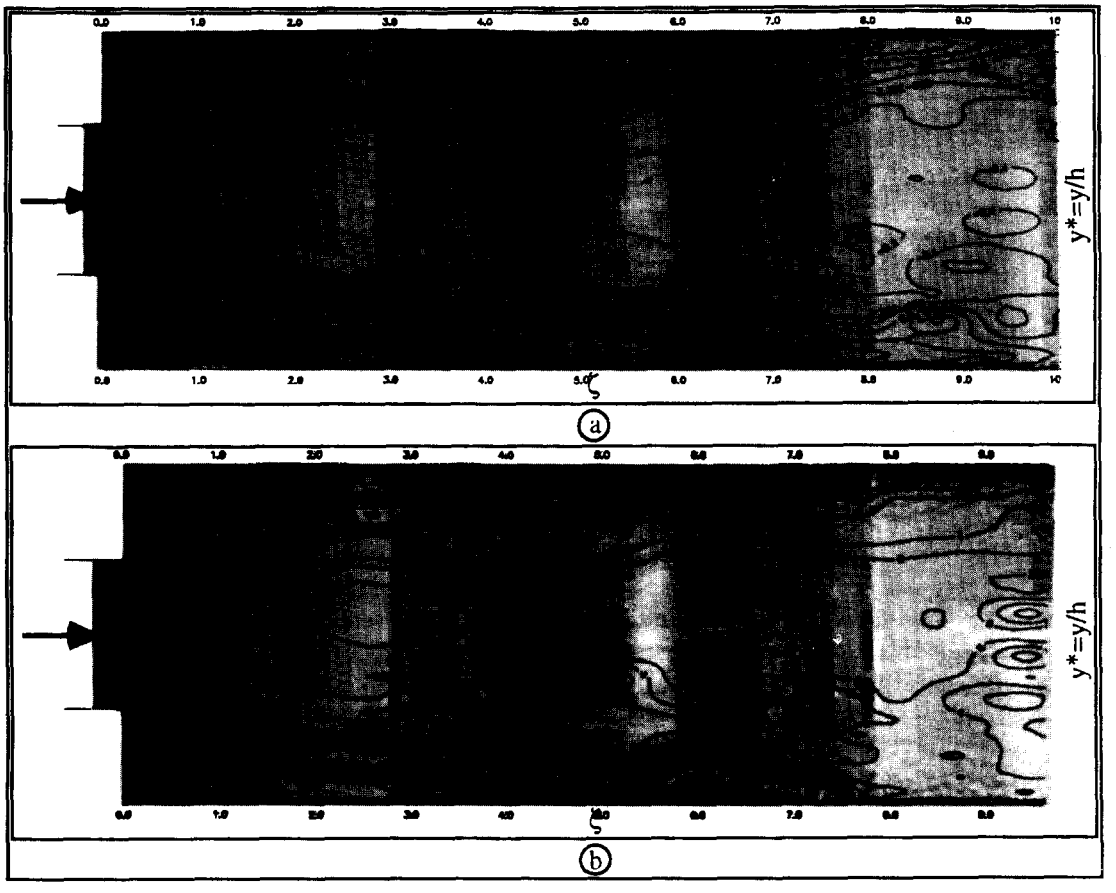

Figure 8. Superposition of the skewness factor contours $\mathscr{S}$ (a) and the flatness factor contours $\mathscr{F}$ (b) to the visualization picture downstream of the sudden expansion for $U_{LSI} = 3.2$ m/s and $x = 26.7\%$.

3.3. *Evolution along the central line*

The decrease of the axial liquid velocity $\bar{u}_L$ and gas velocity $\bar{u}_\ell$ begins at the entrance into the singularity and stabilizes farther away in the vortices regions when the single-phase flow becomes quasi-established again. Outside the recirculation flow, the velocities of the phases decrease progressively up to the establishment of the flow. For example, the variation of $\bar{u}$ along the axis of the expansion for both liquid and gas phases are plotted in figure 9a. Both curves tend towards the asymptote $\bar{u}(\zeta) = \sigma\bar{u}(\zeta = 0)$. The deceleration of the phases is accompanied by an increase of the static pressure which has the tendency of squeezing the bubbles progressively (decrease of volume). In particular, the variation of the diameters ($D_\ell(y = 0,\zeta)$) on the central streamline (axis of the expansion) is plotted in the same figure 9a. The evolution obtained shows that the diameter decreases progressively as one goes farther away from the expansion. This situation is similar to that encountered in axisymmetric sudden expansion (Aloui 1994). The decrease of the diameter cannot be attributed only to the variation of the pressure. If the compression is assumed adiabatic or isothermal, the variation in the size of the bubbles would give only 1% which is much less than the experimental values. This decrease, to a greater extent, is also due to the fragmentation of bubbles along their trajectories. This was observed during the visualization of the flow by fast video camera.

Concerning the fluctuations of the axial velocity, it is observed that the bubbly flow is much more disturbed than the single-phase flow. For example, figure 9b gives the evolution of the standard deviation ($\sqrt{\bar{u}'^2}$) along the axis of the two-dimensional sudden expansion for single phase and two-phase flow. For the liquid phase, one can observe that the gap between single-phase flow and bubbly flow is conserved. This reconfirms the observation already made in the study of flow upstream of the expansion. Effectively, the fluctuations of the liquid velocity in two-phase flow are about four times higher than those in single-phase flow. Whereas for the dispersed phase (bubbles), a slight decrease of the fluctuating velocity is observed as one moves farther away from the expansion. This decrease is almost similar to that of the average axial velocity.

3.4. *Evolution along the side walls*

At a distance of 2 mm from the lateral walls on both sides of the expansion, the variation of the axial velocity of the liquid and bubbles is given in figure 10a. For the liquid phase, there is symmetry of the flow since there is a similarity between the axial velocity profiles $\bar{u}_L$ at $y = -48$ mm and at $y = +48$ mm. As for the dispersed phase (bubbles), one can observe a presence of a few bubbles in the small vortex ($\zeta < 1$). These bubbles have the tendency of going back into the single-phase flow because the signs of $\bar{u}_L$ and $\bar{u}_\ell$ are opposite in the small vortex. At present, there is no explanation for this surprising phenomenon. In the region limited by $1 < \zeta < 7$ (big vortex), the axial velocities in the liquid and gas phases are practically equal, which presents a local no-slip situation between the phases. Beyond $\zeta = 7$ (reattachment point), the local slip between the phases is significant and shows clearly that the velocity of the bubbles is higher than that of the liquid. In the view of these observations, the position of the different vortices can be located. At both sides of the singularity, these vortices are almost identical. The small vortex (located deep down the step) is then of length h (h being the step height) and the big vortex has a size of about $6h$. The latter is located between the small vortex and the reattachment point which is found at $\zeta = 7$. The direction of liquid flow near the wall in the small vortex is the same as that of the main flow, but opposite to the direction of liquid flow in the big vortex.

Near the lateral walls ($y = -48$ mm), the standard deviations ($\sqrt{\bar{u}'^2}$) are plotted in figure 10b for the two phases. In contrast with single-phase flow (Aloui & Souhar 1994), the variation of these standard deviations is almost the same and the regions which contain less bubbles are areas of "low turbulence" as is the case of the small vortex and the reattachment point. This situation, enables once again to locate the small vortex at $\zeta_1 \approx 1$ and the point of reattachment at $\zeta_2 \approx 7$ for the liquid phase and ≈ 7.5 for the bubbles. In the case of fluctuations of axial velocity of bubbles around the reattachment point, one observes the existence of a wide dispersion. This dispersion is mainly due to a very low number of bubbles in the region (bubbles nonexistent), on which the standard deviation does not converge correctly to its presumed value. Thus, taking into consideration the

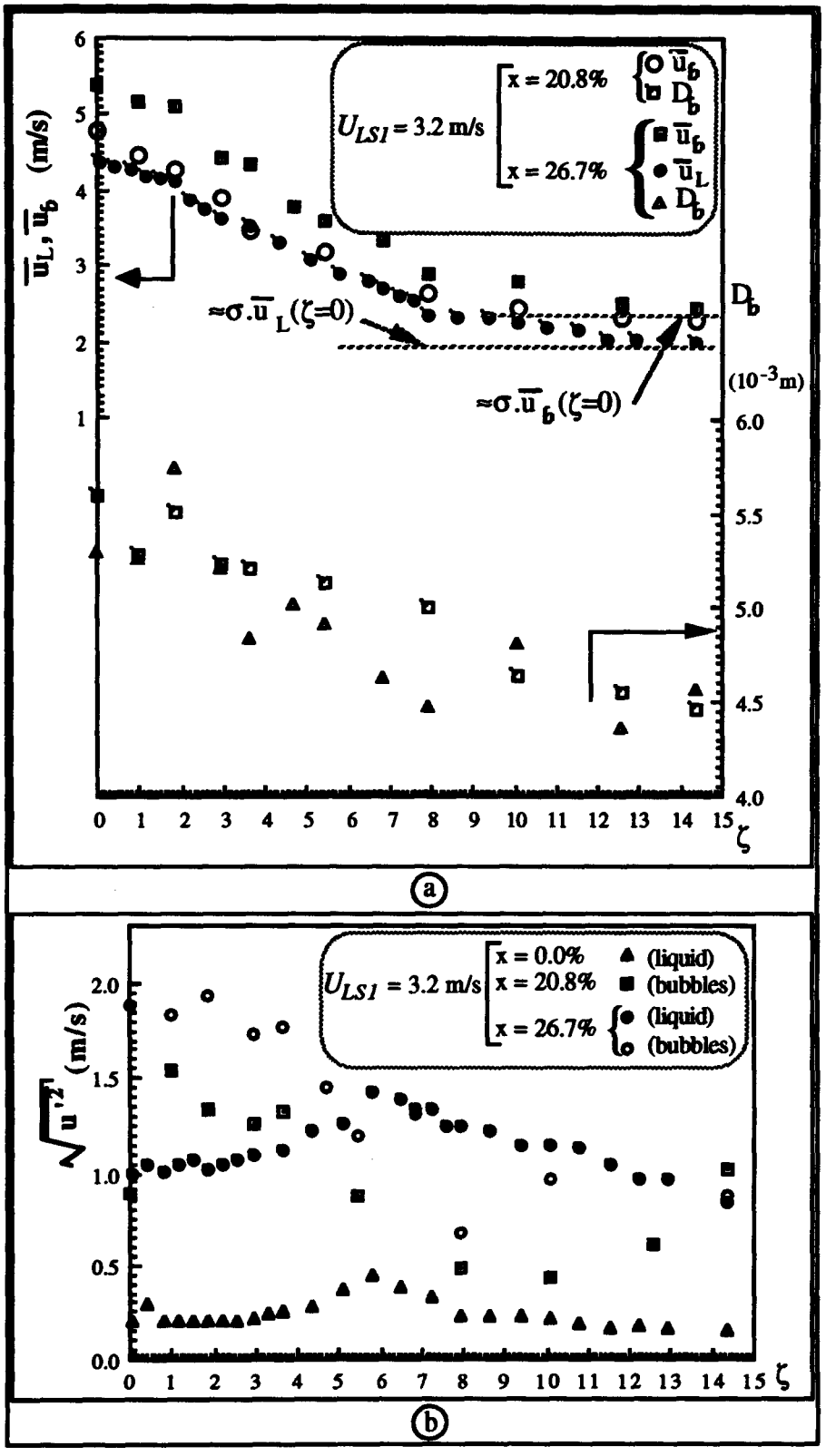

Figure 9. Evolution of the mean and fluctuating axial velocities and the bubbles granulometry along the central line of the sudden expansion.

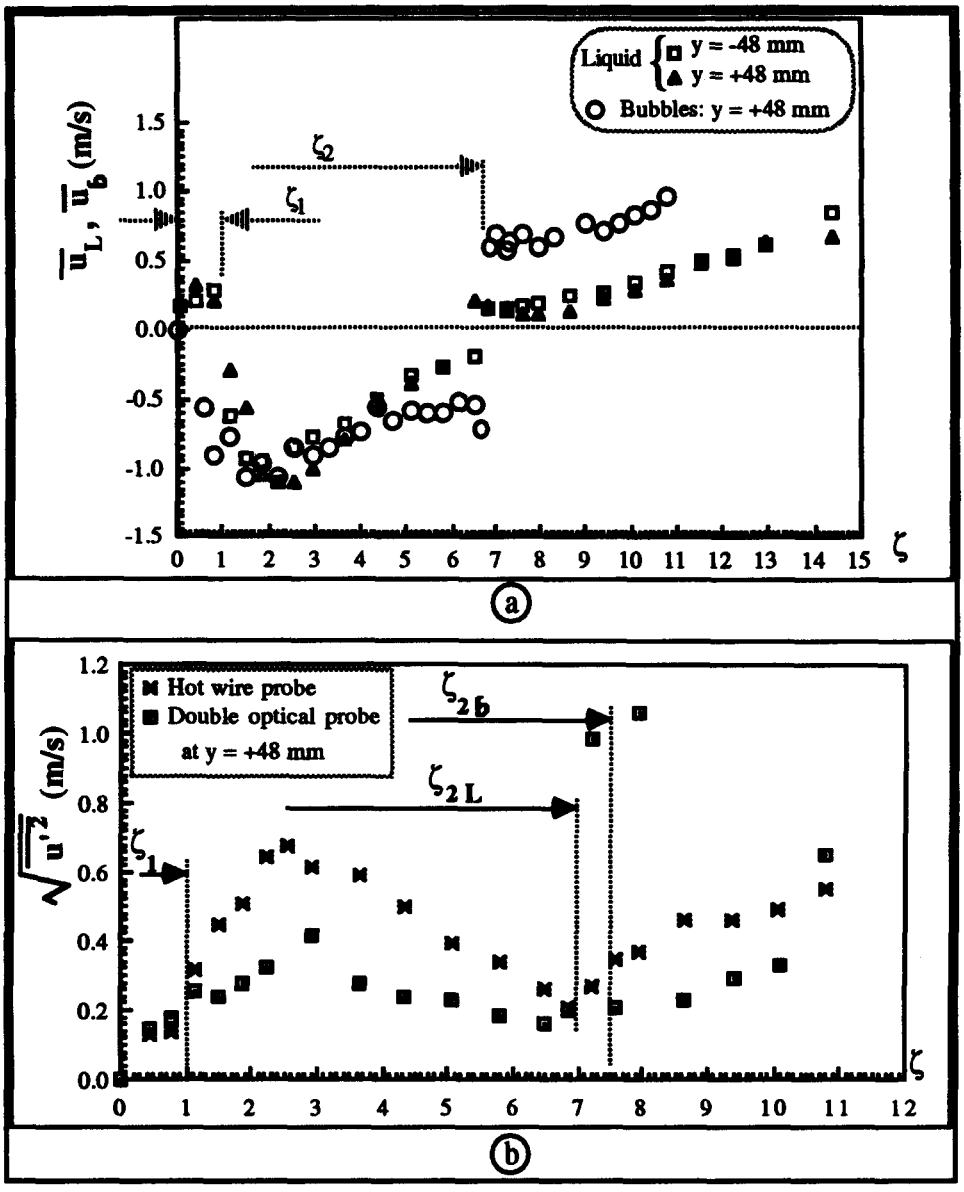

Figure 10. Evolution of the mean and fluctuating axial velocities along the lateral side walls of the sudden expansion for $U_{LSI} = 3.2$ m/s and $x = 20.8\%$: (a) mean axial velocity (b) fluctuating axial velocity.

liquid and gas phases, one can admit that the position of the reattachment point of the bubbly flow is located between 7 and 8 h.

3.5. *Organization diagram of the bubbly flow*

From the different velocity profiles $\bar{u}_L$ and $\bar{u}_b$ obtained, the jet lines in both liquid and dispersed phases were determined by using:

$$\int_{Y_j(\zeta)}^{Y_0} (1 - \varepsilon_2(y,\zeta))\bar{u}_L(y,\zeta)dy = 0 \quad \text{and} \quad \int_{Y_j(\zeta)}^{Y_0} \varepsilon_2(y,\zeta)\bar{u}_d(y,\zeta)dy = 0$$

where Y_0 and $Y_j(\zeta)$ represent the distances at $y = 50$ mm and at y located on the jet line respectively.

The results indicated in figure 11 show that the different jet lines obtained for the liquid phase remain almost the same as those obtained for the dispersed phase. In particular, it is observed that the reattachment point is located between $\zeta = 7$ and $\zeta = 7.5$.

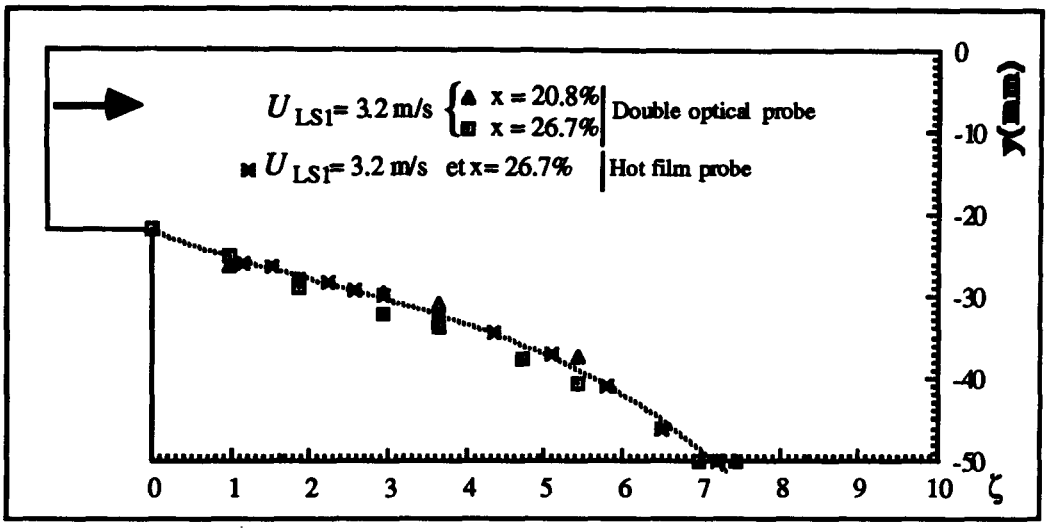

Figure 11. Comparison between the different separation boundaries obtained from the axial velocities of liquid and gas phases.

During the numerical processing of the couples of optical signals, the local average frequency of the bubble passage was determined. The variation of this frequency is similar to that of the local void fraction outside the recirculation regions. Effectively, in the vortex region, there is a mimimum passage frequency. The latter indicates the position where the axial velocities $\bar{u}_\ell$ are nearly zero (figure 12). The positions of the velocities $\bar{u}_\ell = 0$ are equally represented, and thus the points obtained are almost the same and define a straight line (Δ) inclined at about 5° to the lateral wall of the expansion and which represents the axis of the big vortex. The intersection of this line with the wall is located in the vicinity of the reattachment point. The angle of inclination (5°) is of the same order as the one obtained by visualization and by the skewness and the flatness factors during the study of the axial velocity $\bar{u}_L$ in the liquid phase.

The results obtained on the axial velocities $\bar{u}_L$ and $\bar{u}_\ell$ as well as the granulometry of the bubbles lead to the elaboration of a reorganization diagram of the two-phase flow downstream of the sudden expansion (figure 13). The bubbly flow obtained is divided into two regions: a principal flow and a recirculation flow. In the recirculating region, there are two counter-rotative vortices with different sizes. The direction of flow at the wall in the big vortex is opposite to the main flow.

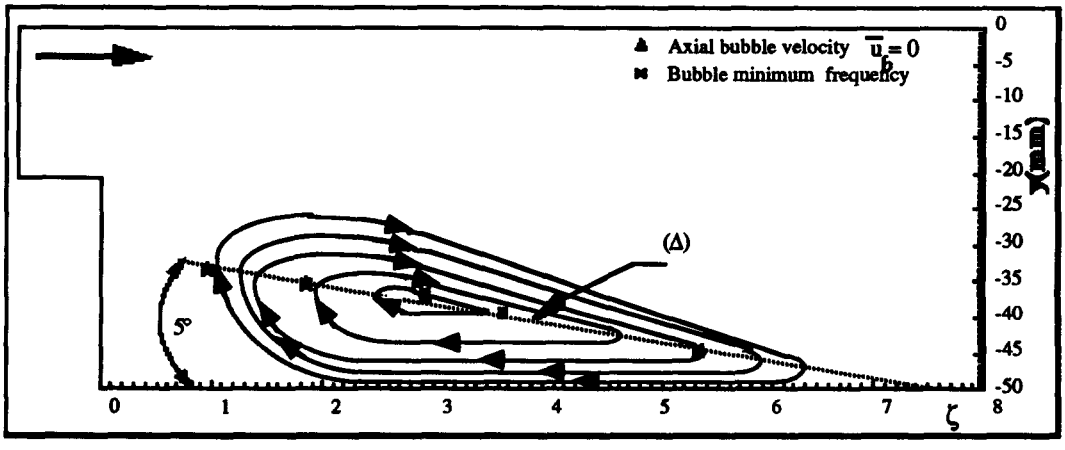

Figure 12. Position of zero axial velocity and the very low frequency passage of the bubbles in the big vortex for $U_{LSI} = 3.2$ m/s and $x = 20.8\%$.

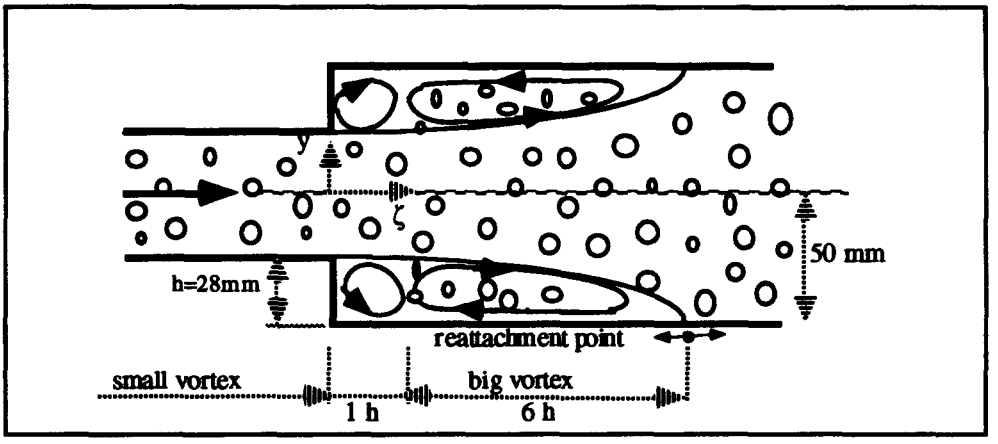

Figure 13. Reorganization of the bubbly flow downstream of the flat sudden expansion.

4. CONCLUSION

The experimental study presented here brings several data concerning the dynamic of bubbly flow in flat duct symmetric sudden expansion. These data, composed of the average and fluctuating velocities relative to each phase and the granulometry, are very useful for future numerical simulation. For different flowrates explored, a symmetrical bubbly flow was chosen. Experimental data were presented and their characteristics were discussed. The following results were obtained.

1. The results of the average velocities relative to each phase downstream and near the wall have allowed the determination of different lengths that characterize the recirculating zone as well as their boundaries with the main flow. Especially, the reattachment point has been located at about 7.5 step height.
2. The slip velocities found are very high compared with classical values obtained in bubbly flow. This is due to our particular geometric configuration where the pressure gradients are very high.
3. The fluctuation rates for each phase are about four times higher than those of liquid single phase; and the high order moments (skewness and flatness factors) are very different to the classical values obtained in turbulent single phase flow.
4. The contour plots of the skewness factor and the flatness factor relative to the continuous phase (liquid) reflect perfectly the closed stream lines in the big vortices.
5. The size of bubbles decreases along their trajectories. This decrease is due to the pressure increase and mainly to the fragmentation which was visualized by the fast video camera.

Acknowledgements—The authors would like to thank the two anonymous referees whose comments greatly improved the presentation. This research was supported by CNRS and Gredic Diphasique GDR 1027. This support is gratefully acknowledged.

REFERENCES

Aloui, F. 1994 Etude des écoulements monophasiques et diphasiques dans les élargissements brusques axisymétrique et bidimensionnel. Ph.D. thesis, INPL, Nancy, France.

Aloui, F. & Souhar, M. 1994 Etude de la chute de pression singulière dans les élargissements brusques en écoulement monophasique turbulent. *J. Appl. Mathematics Physics (ZAMP)* **45**, 371–386.

Belakhovsky, M. 1966 Eléments d'une description statistique d'un écoulement diphasique—écoulement eau-air à bulles. *C.E.N-G.* Note interne TT No. 226, April, France.

Bel Fdhila, R. 1991 Analyse expérimentale et modélisation d'un écoulement vertical à bulles dans un élargissement brusque. Ph.D. thesis, INPT, Toulouse, France.

Bel Fdhila, R. & Simonin, O. 1992 Modélisation des écoulements turbulents à bulles: application à un élargissement brusque en conduite verticale. EDF/LNH—Groupe Méca. Fluides Industrielles, ARD-AID no. E4404R, Chatou, France.

Clark, N. N. & Turton, R. 1988 Chord length distributions related to bubble size distributions in multiphase flows. *Int. J. Multiphase Flow* **14,** 413–424.

Galaup, J. P. 1975. Contribution à l'étude des méthodes de mesure en écoulement diphasique. Ph.D. thesis, Grenoble, France.

Herringe, R. A. & Davis, M. R. 1976 Structural development of gas–liquid mixture flows. *J. Fluid Mech.* **73,** 97–123.

Liu, T. J. 1993 Bubble size and entrance length effects on void development in vertical channel. *Int. J. Multiphase Flow* **19,** 99–113.